Conformational Partitioning of the Fusion Peptide of HIV-1 gp41 and Its Structural Analogs in Bilayer Membranes

Michael W. Maddox and Marjorie L. Longo
Department of Chemical Engineering and Materials Science, University of California, Davis, California 95616 USA

ABSTRACT Experiments have shown that the ability of the HIV-1 virus to infect cells can be greatly diminished by deactivation of the N-terminal (fusion) peptide of its glycoprotein gp41. Deactivation can be achieved by the deletion of several amino acid residues, or replacement of a hydrophobic residue with a polar residue, to form mutant variants of the wild-type peptide. We report Monte Carlo simulation studies of a simplified peptide/membrane model, representing the interaction of an HIV-1 fusion peptide (FP) and four closely related mutagens with a lipid bilayer. In agreement with experimental results, we show that FP inserts deeply into the bilayer at $\sim 40°$ to the bilayer normal. We also show a previously unreported behavior of membrane peptides, namely their equilibrium partitioning between several distinct conformations within the bilayer. We quantify this partitioning behavior and characterize each conformation in terms of its geometry, energy, and entropy. The diminished ability of FP mutagens to hemolyse and aggregate red blood cells due to their partitioning into unfavorable conformations, is also discussed. Our analysis supports a negative curvature mechanism for red blood cell hemolysis by FP. We also suggest that the small repulsive forces between surface-adsorbed peptides in opposing membrane surfaces may block aggregation.

INTRODUCTION

The HIV-1 virus infects host cells by first attaching itself to a cell receptor via the glycoprotein gp120,000 (gp120). This is followed by activation of the N-terminal peptide of glycoprotein gp41,000 (gp41), which inserts deeply into the cell bilayer, causing fusion between the target cell and the HIV-1 viral envelope (Gordon et al., 1992). Site-directed mutagenesis studies have shown that modifications to the N-terminal fusion peptide of gp41 can seriously disrupt the fusion process, rendering HIV-1 inactive (Freed et al., 1990; Buchschacher et al., 1995; Schaal et al., 1995). Synthetic peptides based on the N-terminal region of gp41 behave in a similar manner and therefore appear to be good models for investigating the activity of the entire HIV-1 virus. Wild-type synthetic peptides can lyse membranes, induce pore formation and leakage in lipid vesicles, and effect cell aggregation, whereas many mutated variants are inactive or exhibit greatly reduced activity (Martin et al., 1996; Pereira et al., 1997; Mobley et al., 1999). Experimental investigations of synthetic N-terminal peptides of gp41 have shown a deeply inserted, largely α-helical structure at low peptide-to-lipid concentrations, which changes to a β-sheet-like secondary structure at higher concentrations (Gordon et al., 1992; Mobley et al., 1999). In contrast, peptide mutants tend to lie closer to the cell bilayer surface, although most still show an α-helical to β-sheet conversion with increasing peptide-to-lipid concentration (Mobley et al., 1999). Peptide variants include replacement mutants in which a single hydrophobic amino acid residue has been replaced by a polar residue, and deletion mutants, in which one or more residues have been deleted. The activity of the wild-type peptide increases with peptide concentration, but this increase is not simply a consequence of the accompanying change in secondary structure, because α-helix to β-sheet conversion is also observed in inactive variants (Martin et al., 1996; Pereira et al., 1997; Mobley et al., 1999).

The functional activities of the 23-residue wild-type N-terminal fusion peptide of gp41, and several mutated variants were recently investigated in a series of experiments (Mobley et al., 1999). Measurements were made to determine the extent to which each peptide could hemolyse human erythrocytes and aggregate erythrocytes, at 310 K and pH 7.4. (Fusion of resealed erythrocyte ghosts was also reported, but it is possible that the mixing of cell contents in this type of assay occurs by a mechanism other than fusion.) For each process, the peptide variants showed reduced functional activity, but the extent of the reduction varied depending on the specific peptide mutation. This suggests that a more detailed study of the insertion behavior of FP and its variants could provide important information regarding the mechanisms of specific cell processes.

In recent years, computer simulation has become an invaluable research tool, complimenting experimental methods in almost every scientific discipline. Although no molecular model can perfectly reproduce a real system, the molecular-level detail that such models afford can nevertheless provide crucial insights into microscopic behavior. Such detail is much harder if not impossible to obtain experimentally. Using one such computer simulation technique (Maddox and Longo, 2002), we have probed the conformational behavior of FP and its variants in a phospholipid membrane, searching for structural clues to the changes in biological activity effected by small variations in

Submitted May 8, 2002, and accepted for publication August 21, 2002.

Address reprint requests to Marjorie L. Longo, Department of Chemical Engineering and Materials Science, University of California Davis, One Shields Avenue, Davis, CA 95616. Tel.: 530-754-6348; Fax: 530-752-1031; E-mail: mllongo@ucdavis.edu.

0006-3495/02/12/3088/09 $2.00

the wild-type FP peptide sequence. Our model shows that FP inserts deeply into the membrane, lies at an oblique angle to the surface, and is in a largely α-helical form at low concentration in agreement with previous results (Mobley et al., 1999). We predict, however, that rather than effecting a wholesale conformational change, the peptide mutations cause a partitioning between several different conformational states (a conformational state is a distinct set of closely related conformations), including the fully inserted (fi) state preferred by the wild-type peptide. We have characterized these conformational states and quantified the conformational partitioning of each peptide. Although rarely mentioned in experimental studies, due to the difficulty in resolving the closely related structures, conformational partitioning could be an extremely important effect that impacts many cell processes. It may help to explain certain mechanistic behaviors, the partial reduction of activity for mutagens, and a host of other peptide/bilayer effects. In the Discussion, we use the conformational and partitioning information from our simulations to provide insights into the mechanisms by which hemolysis proceeds and by which aggregation may be blocked.

METHODS

A complete description of the peptide/bilayer model, residue parameter set (hydropathy scale), and Monte Carlo method used here is presented in our earlier study of peptide insertion into lipid bilayers (Maddox and Longo, 2002) but can be summarized as follows. The peptide is modeled as a linked chain of hard spheres that interact with a mean field approximation of a lipid bilayer membrane. The interaction is described by three energy fields characterized by residue-dependent semiempirical parameters. The fields represent the hydrophobic effect, the polar energy of fully or partially charged amino acids, and the energy due to hydrogen bonding. In addition, the internal hydrogen bonding along the peptide backbone is a function of the helicity of the peptide chain. The combined effect of these system characteristics can be summarized as follows; a peptide chain favors a random coil in the aqueous phase (ap) when it has no interaction with the bilayer. In close proximity to the surface, all peptides reversibly adsorb into the bilayer interface region (the lipid head region). Although polar interactions involving residue side-chains are maintained in the interface, a water content gradient exists that encourages peptides to self-assemble into a helical secondary structure. Hydrophobic helical segments of the peptide can pass freely into the hydrophobic bilayer interior, but the loss of polar interactions in the interior provides an energy barrier to the passage of polar segments. The four residues at each end of a peptide also experience an energy barrier to insertion into the bilayer interior due to their incomplete internal hydrogen bonding even in a helical arrangement.

Unlike the peptides we modeled previously, FP and its variants are carboxyamidated, requiring a slight adjustment to our peptide model. Although the extra amine group should not be modeled as an additional amino acid residue, it does have a potentially important effect on the internal hydrogen bonding at the carboxyamidated end. Therefore, it is accounted for by the addition of an extra hard sphere at the carboxyamidated end of the peptide model. This "amine sphere" possesses one-half of the hydrogen bonding properties of a regular amino acid residue but has no hydrophobic or polar interactions with the lipid bilayer, i.e., $H_0 = -3.06$ kcal/mol, $b_0 = 0.0$, $b_1 = 0$, and $q_0 = 0$.

The energy of the system is minimized using the Monte Carlo simulation technique, and all simulations were performed on a Microway Screamer-LX SuperCache-8 workstation with a 667-MHz DEC alpha 21164 CPU (Microway, Kingston, MA).

It should be noted that our model is not expected to reproduce the adsorption behavior of large proteins that are globular in the ap, effectively forming their own internal hydrophobic domain.

The amino acid sequence of FP, the carboxyamidated N-terminal peptide of HIV-1 gp41 (residues 519–541), and the sequences of the FP variants are shown below (Mobley et al., 1999).

FP:
NH_2–A V G I G A L F L G F L G A A G **S T M** G A **R S**–$CONH_2$
FP520V/E:
NH_2–A ***E*** G I G A L F L G F L G A A G **S T M** G A **R S**–$CONH_2$
FP529F/Y:
NH_2–A V G I G A L F L G ***Y*** L G A A G **S T M** G A **R S**–$CONH_2$
FP527L/R:
NH_2–A V G I G A L F ***R*** G F L G A A G **S T M** G A **R S**–$CONH_2$
FPCLP1:
NH2–F L G F L G A A G **S T M** G A **R S**–$CONH_2$

All residues are indicated by their one letter codes, residues with polar side-chains ($q_0 < 0$; Maddox and Longo, 2002) are shown in bold type, and replacement residues are underlined. Residue number 541 is located at the carboxyamidated end in all cases.

The interaction of a single peptide chain with a 36-Å lipid bilayer was modeled in each simulation run. A single run consisted of 600 million system configurations for FP529F/Y, FP527L/R, and FPCLP1, and 300 million for FP and FP520V/E. Shorter runs were used for the latter two peptides due to their greater conformational stability in the membrane. All simulations were performed at 305 K and pH 7, and 10 runs were completed for each peptide. The polarity factor (f_q) for the bilayer tail region was 0.85, corresponding to a polarity somewhere between those of octanol and hexadecane, as suggested by experimental studies (Roseman, 1988; Griffith et al., 1974) and our earlier simulation work (Maddox and Longo, 2002).

The first 30 million configurations of each simulation run were discarded so that data were only collected for the fully equilibrated system. Adequate equilibration was demonstrated by collecting data over the rest of the 600 million configuration run in 19 separate blocks of 30 million configurations and calculating the standard deviation of several quantities, primarily the total energy of the system. For the peptides that did not desorb from the bilayer after the initial equilibration period (FP, FP520V/E, and FP529F/Y), the standard deviation was less than 0.5% of the average total energy. Such a small variation in total energy shows that the system was stable throughout the run and therefore fully equilibrated. The peptides that periodically desorbed from the bilayer (FP527L/R and FPCLP1) showed greater variations in total energy (standard deviations of 4% and 10%, respectively) due to the very large energy difference between ap and membrane conformations. However, no energetic drift was observed within the 19 blocks of any of the 10 simulation runs for either of these peptides, and inspection of the peptide trajectories clearly showed that the conformational changes (including desorption) were reversible, typically occurring several times within each simulation run. Therefore, it is reasonable to conclude, even for these two peptides, that the systems had equilibrated during the discarded 30 million configurations, even though the equilibrated system was quite dynamic.

To ensure that the results were independent of the initial configuration, two different initial configurations were used for each peptide. A random coil in the ap was used in the first five simulation runs and a *tb* helix in the remaining five. After the equilibration period, all 10 systems were statistically indistinguishable regardless of their initial configuration. We conclude that the simulation results are independent of the initial peptide configuration.

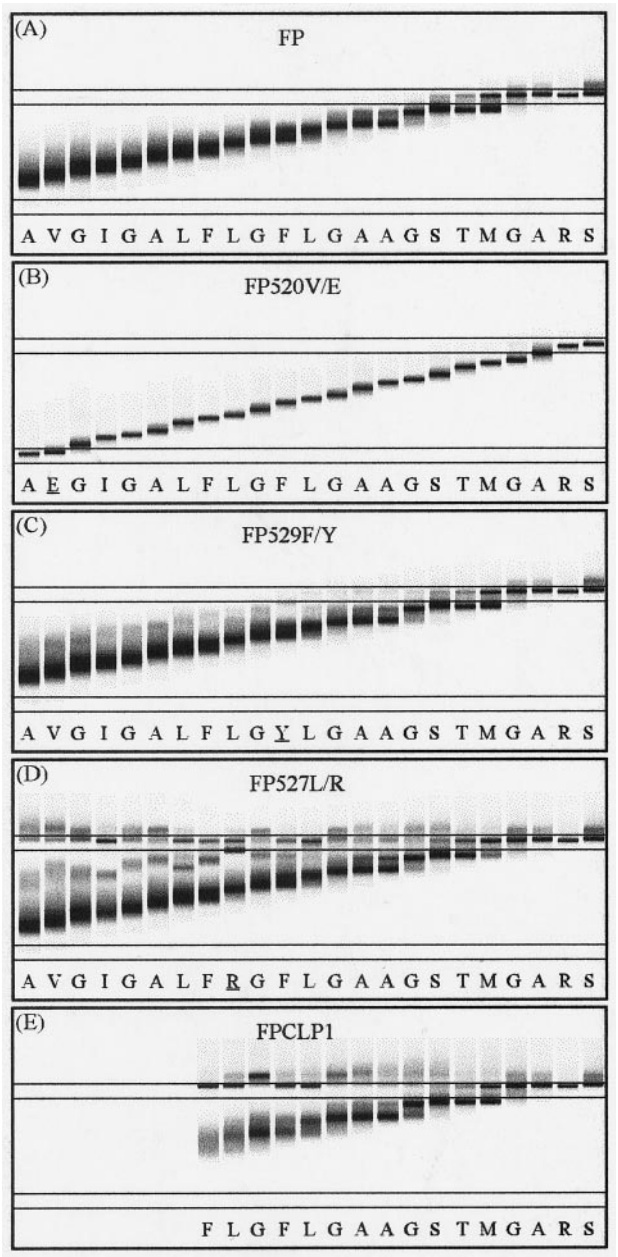

FIGURE 1 Probability distribution functions for every residue of FP and the four FP variants. Darker regions indicate higher probability. The two bilayer interface regions (one at each side of the membrane) are indicated by the closely spaced parallel lines, and the bilayer interior is in between.

RESULTS

Throughout the simulation runs, the depth of insertion of every residue was monitored and probability distribution plots constructed for each one. These data are presented in Fig. 1. For each peptide, the residues are indicated along the horizontal axis, and the probability distributions are plotted vertically. Darker bands indicate a greater probability of finding a residue at a particular position and therefore indicate the favored depth of insertion of each residue within the bilayer. The two sets of parallel horizontal lines indicate the positions of the bilayer interface regions, and the region in between is the bilayer interior. It should be noted that although a great deal of information is contained within these figures, the angle of insertion is not, because the horizontal axis is unrelated to the (x, y) positions of residues in the membrane.

In Fig. 1, *D* and *E*, more than one peak (dark band) is evident for most of the residues, indicating the existence of more than one stable residue position after equilibration. This suggests that more than one stable conformational state exists for these peptides (a conformational state is a set of similar conformations that can be grouped together). In fact, close inspection of the data reveals that all of the peptides have more than one stable conformational state, although one is often heavily favored over the others. By following the trajectory of every residue during each simulation run, peptides can be observed flipping back and forth between different conformational states, even after complete equilibration of the system. This type of reversible conformational change for a single peptide during a long simulation run corresponds to a partitioning over conformational states for peptides in a dilute multipeptide system (peptide-peptide interactions are negligible). Furthermore, the proportion of time that a single peptide spends in each conformational state during a sufficiently long simulation run is equal to the proportion of peptides in each conformational state in a dilute multipeptide system.

Although each peptide has between two and five different conformational states, some are common to more than one peptide. Conformational states for different peptides were considered to be the same if the probability distribution peaks were identical for all equivalent residues. In total, six unique conformational states were observed for FP and its variants. One of these states includes all random coil conformations in the ap, whereas the other five are membrane-bound and can be described as surface adsorbed (sa), partially inserted (pi) from residue 527 (527pi), pi from residue 529 (529pi), fi, and tb. Representative conformations (the most likely single conformation within a conformational state) of each membrane-bound state, taken directly from simulations, are shown in Fig. 2. The N-terminal residue is white, and the C-terminal residue is black. Because all residues in the model are the same size, the smaller residues in Fig. 2 indicate greater distance from the observer.

The angle of insertion and length of each peptide (and peptide segments) were also monitored throughout each simulation, and a series of angle and length distribution functions generated. The distribution functions were then deconvoluted to produce angle and length distributions for each conformational state. Table 1 shows the angles of insertion, and Table 2 shows the corresponding lengths.

Using the data reported above, we can characterize the five membrane-bound conformational states. The sa conformation is loosely helical but not fully extended (the end-to-

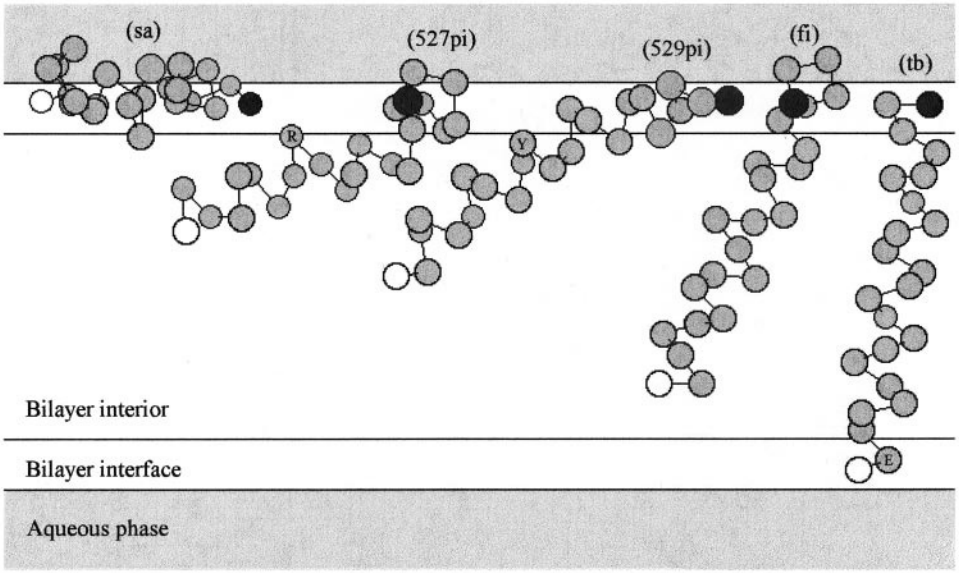

FIGURE 2 Representative snapshots of the five membrane conformational states observed for FP and its variants; sa, surface adsorbed; 527pi, partially inserted, tethered at residue 527; 529pi, partially inserted, tethered at residue 529; fi, fully inserted; tb, *trans*-bilayer. The N-terminal residue is indicated by a white circle and the C-terminal residue by a black circle. The conformational states, 527pi, 529pi, are specific to FP527L/R and FP529F/Y, respectively, so the replacement residue is indicated in each case. Although several peptides partition into the tb state, only FP520V/E favors this conformation over all others. The replacement residue for FP520V/E is therefore indicated in the tb figure.

end separation is widely distributed about an average length of ~22 Å, whereas the fully extended helix is ~33 Å long). The residues are generally located in the bilayer interface with all segments of the peptide roughly parallel to the bilayer surface. There is a good deal of flexibility, however, and the 15° standard deviation in the insertion angle indicates that both ends can reversibly insert into the bilayer interior and also reversibly desorb from the bilayer surface.

The pi conformational states (527pi and 529pi) differ only in the residue that tethers the hydrophobic tail to the bilayer interface. Both have a loosely helical polar segment that lies in the bilayer interface, parallel to the bilayer surface, and both have helical, hydrophobic tails that insert obliquely into the bilayer interior from a tethering polar residue. The tethering residue at position 529 yields a slightly longer tail segment, which can insert more deeply, and at a smaller insertion angle (52° for 529pi, 65° for 527pi).

The hydrophobic tail segment of the fi conformation is an extended helix, inserted deeply into the bilayer interior at an angle of 38° to the bilayer normal. It is quite flexible; the angle of insertion has a standard deviation of 13°, and the depth of insertion of the N-terminal residue has a standard deviation of ~6 Å. The polar segment is loosely helical and is also inclined into the bilayer interior but at a greater angle from the bilayer normal than the hydrophobic tail (55°).

The tb conformation is the most rigid, the terminal residues being tethered in opposite bilayer interface regions. To span the bilayer, this conformation has only a slight kink between its hydrophobic and polar segments and is largely helical throughout. Its insertion angle is close to the bilayer normal (16°). This angle is somewhat dependent on the ratio of bilayer thickness to peptide length and can be larger for a longer peptide or narrower bilayer. However, for a shorter peptide or thicker bilayer, the *tb* conformation is not oriented closer to the bilayer normal as might be expected.

TABLE 1 Angle of insertion of entire peptide and peptide segments for the five membrane conformational states of FP and variants

Conformational state	Full peptide	Hydrophobic tail segment (AVGIGALFLGFLGAAGS)	Polar head segment (STMGARS)
tb	16 ± 6°	17 ± 7°	23 ± 11°
fi	38 ± 13°	34 ± 13°	55 ± 18°
529pi	51 ± 18°	52 ± 10°	88 ± 18°
527pi	67 ± 10°	65 ± 12°	87 ± 20°
sa	90 ± 15°	89 ± 15°	87 ± 20°

Each angle is the peak of the appropriate angle distribution function ± 1 SD. All angles are measured from the perpendicular to the bilayer surface.

TABLE 2 Length of entire peptide and peptide segments for the five membrane conformational states of FP and variants

Conformational state	Full peptide	Hydrophobic tail segment (AVGIGALFLGFLGAAGS)	Polar head segment (STMGARS)
tb	33.4 ± 0.6 Å	24.5 ± 0.5 Å	9.8 ± 0.4 Å
fi	33.1 ± 1.5 Å	24.4 ± 0.5 Å	9.8 ± 1.2 Å
529pi	28.2 ± 4.3 Å	24.8 ± 1.2 Å	9.8 ± 2.0 Å
527pi	~32 ± 3 Å	24.8 ± 0.9 Å	9.8 ± 2.2 Å
sa	~22 ± 8 Å	19.3 ± 5.6 Å	~6.5 ± 1.5 Å

Each length is the peak of the appropriate length distribution function ± 1 SD.

Instead, the peptide favors conformations that do not span the bilayer such as the fi or sa conformations.

Having identified and characterized the available conformational states, careful analysis of the probability distribution data allowed us to quantify the conformational partitioning of each peptide. These data are given in Table 3. It should be noted that by limiting the size of the ap within the simulation box (77 Å on each side of the bilayer), and equilibrating each peptide/membrane system before taking data, diffusion-limited partitioning of the peptide between the aqueous solution and the membrane is minimized in our model. By limiting peptide diffusion in the ap, random contact with the membrane surface occurs more frequently, and partitioning between bilayer and ap conformations is energetically limited rather than diffusion limited. This may result in a slight underestimation of the proportion of FP527L/R and FPCLP1 in the ap conformational state when compared with experimental results.

The observed conformational partitioning is a result of the small Gibbs energy differences (ΔG) between conformational states. In a computer simulation, each configuration (snap-shot) represents a single quantum energy state of the system with a specific internal energy, U. The system partitions between these quantum states according to the Boltzmann distribution,

$$\frac{N_a}{N_0} = e^{\frac{-\Delta U}{RT}} \tag{1}$$

in which N_0 is the population of the ground state (U_0), N_a is the population of quantum state a (U_a), and $\Delta U = U_a - U_0$. Although a smaller ΔU means a higher population for a specific quantum energy state, it does not ensure a higher population for a conformational state. This is because conformational states comprise a large number of quantum energy states grouped together. The total population of a conformational state is, therefore, the sum of the populations of each individual quantum energy state within the group. This quasidegeneracy is directly related to ΔS, the entropy difference between conformational states a and b, by,

$$\Delta S = R \ln W \tag{2}$$

in which $W = q_a/q_b$ (q_a is the number of quantum energy states in conformational state a). The partitioning over conformational states therefore depends on ΔU, T, and ΔS, i.e., it is a function of ΔG. (Although ΔU, T, and ΔS actually give the Helmholtz energy difference, ΔA, rather than ΔG, these quantities are equivalent for a constant volume system, such as ours). As a result, if all quantum energy states within a conformational state are grouped together into a single conformational energy state with average internal energy, U, the system partitions between conformational energy states according to the Boltzmann distribution, providing we use ΔG rather than ΔU in Eq. 1. This is much more convenient for our purposes, because conformational states can have millions of individual quantum energy states.

It should be noted that the Boltzmann distribution describes the partitioning between accessible conformational states only. Inaccessible conformational states are those that are separated from all accessible states by a large, insurmountable energy barrier (high G intermediate conformation). For example, a translocated fi conformational state has the same G, U, and S as its regular counterpart but remains unpopulated by FP and variants. This is because it is inaccessible from any accessible conformational state. To

TABLE 3 The partitioning of FP and its variants into particular conformational states

	% in aqueous phase (ap)	% surface adsorbed (sa)	% partially inserted (pi)	% fully inserted (fi)	% trans-bilayer (tb)
FP	—	—	—	97.9 ± 0.3	2.0 ± 0.3
FP520V/E	—	0.6 ± 1.5	—	14.6 ± 0.8	84.8 ± 1.5
FP529F/Y	0.2 ± 0.3	0.8 ± 1.0	11.4 ± 0.5	86.0 ± 1.3	1.6 ± 0.2
FP527L/R	4.8 ± 1.9	19.2 ± 8.6	15.2 ± 1.9	59.8 ± 9.3	1.1 ± 0.2
FPCLP1	22.6 ± 4.2	23.9 ± 4.3	—	53.5 ± 8.4	—

Each value is the mean of 10 simulation runs ± 1 SD.

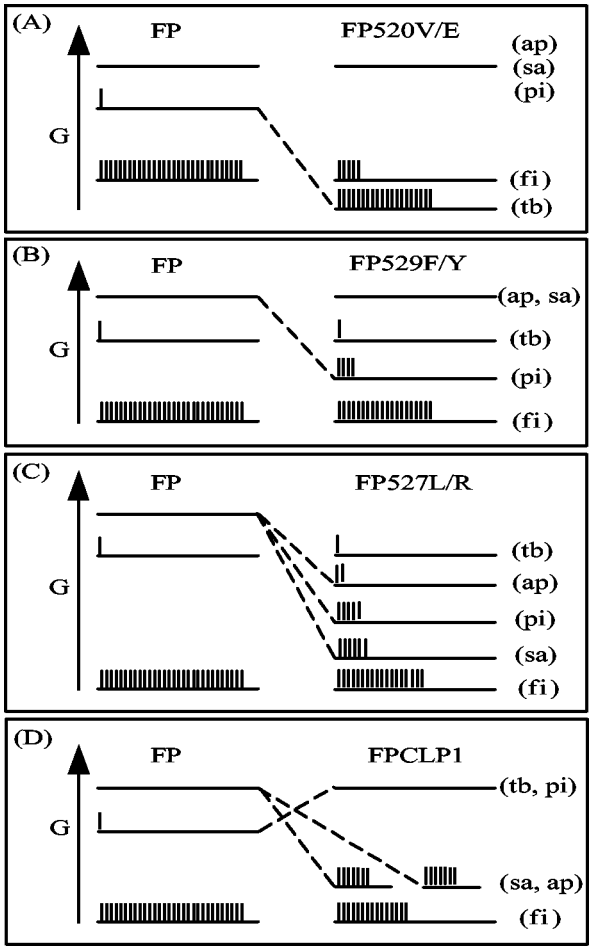

FIGURE 3 Gibbs energy level diagrams (not to scale) illustrating the conformational partitioning of wild-type FP and its variants. The energy level corresponding to a particular conformational state is labeled parenthetically as follows; ap, aqueous phase; sa, surface adsorbed; pi, partially inserted; fi, fully inserted; tb, *trans*-bilayer. Although each conformational state comprises a large number of closely related conformations, and therefore a distribution of quantum energy levels, only the energy levels of the representative conformations for each state are shown. The groups of small vertical lines represent the relative population of each energy level (i.e., the partitioning) at equilibrium. Although the absolute Gibbs energy of the fi state is different for each peptide, all fi states are shown at the same energy level in the figure to illustrate the relative energy changes of the other conformational states.

take up this conformation, the peptide must first translocate across the membrane. In doing so, the polar segment of the peptide enters the bilayer interior, producing a very high-energy intermediate conformation. Such a conformation will remain unpopulated according to the Boltzmann distribution, thereby representing an insurmountable energetic barrier to any translocated conformations. These conformations will therefore remain unpopulated.

Fig. 3 shows Gibbs energy diagrams for the peptide variants in comparison with FP. As noted, each conformational state is reduced to a single energy level.

FP is shown on the left in each part of Fig. 3. The lowest energy level (ground state) is the fi conformational state, the next highest is the tb, and the highest energy level represents all unpopulated conformational states, including pi, sa, and random coil in the ap. The absolute Gibbs energy of the fi conformational state is different for each peptide, but they are set equal in each part of Fig. 3 to illustrate the relative changes of the other energy levels (i.e., the G scale is shifted for each variant). A dashed line indicates the change in energy, relative to fi, of a conformational state upon mutation of FP.

Although the ground state is 98% populated for FP, the tb energy level is also occupied, accounting for the remaining 2% of the total population. Because $N_{tb}/N_{fi} = 0.02$, $\Delta G_{tb-fi} = 2.4$ kcal/mol between fi and tb. In addition, internal energy distributions, taken during all simulations, show that $\Delta U_{tb-fi} = -3.3$ kcal/mol (i.e., U_{tb} is less than U_{fi}). Therefore, the entropy difference between these conformational states, $\Delta S_{tb-fi} = -19$ cal/mol/K. This shows that merely comparing internal energies of different conformations is insufficient to determine conformational stability, and that entropy must also be included. ΔG, ΔU, and ΔS can be found in a similar manner for the transition from fi to every other populated conformational state for each peptide. These data are given in Table 4 for all energy levels at least 1% populated by FP and variants. For energy levels with finite populations of $<1\%$, ΔG is instead calculated from ΔU and an estimate of ΔS. These values are in parentheses in the table.

Fig. 3 *A* shows the effect of replacing a V residue with an E, at position 520. The tb conformation is stabilized relative to fi to such an extent that it becomes the ground state conformation. ΔG_{tb-fi} is negative, and the tb state has a higher population than the fi state. The calculated entropy difference, $\Delta S = -19$ cal/mol/K, is in agreement with the tb − fi value for FP. This is to be expected, because the entropy depends on the number of quantum energy states within a conformational state rather than the internal energy. All other conformational states remain unpopulated.

Fig. 3 *B* shows the effect of replacing an *F* residue with a *Y* at position 529. The tb energy level remains fixed, relative to the fi ground state, and is therefore similarly populated to its FP counterpart, but the pi conformation is stabilized by the polar Y residue. Although ΔU_{pi-fi} is large and positive for this conformation, ΔS_{pi-fi} is also large and positive, so that although ΔG_{pi-fi} is positive, it is small enough to allow significant population of the pi state. Because the tethering of the pi conformation might be expected to restrict the freedom of the inserted hydrophobic segment, it is somewhat surprising that the pi conformational state has significantly higher entropy than the fi state. However, the polar end of the pi conformation does not anchor the peptide in the interface, but instead samples both the bilayer interior and the ap, and the tethering also causes a longer segment of the peptide to remain in a less helical

TABLE 4 Approximate ΔG, ΔU, and ΔS between the fi and other populated conformational states

	ap–fi	sa–fi	pi–fi	tb–fi
FP	—	—	—	2.4, −3.3, −0.019
FP520V/E	—	(3.9, 40.8, 0.121)	—	−1.1, −6.8, −0.019
FP529F/Y	(4.4, 45.9, 0.136)	(3.7, 40.6, 0.121)	1.2, 14.8, 0.044	2.4, −3.3, −0.019
FP527L/R	1.5, 43.0, 0.136	0.7, 37.5, 0.121	0.8, 14.0, 0.043	2.4, −3.3, −0.019
FPCLP1	0.5, 28.1, 0.091	0.5, 24.1, 0.077	—	—

ΔG is calculated directly from partitioning data for populations of ≥1%. For populations <1%, the standard deviation is typically larger than the partitioning percentage, leading to large errors in the calculation of ΔG. Therefore, ΔG is calculated from ΔU and ΔS in these cases (shown in parentheses). Energy differences are given in kcal/mol, entropy differences in kcal/mol/K.

and therefore more disordered state in the interface region. These effects together account for the observed entropy difference. ΔG_{sa-fi} and ΔG_{ap-fi} are large and positive, and the sa and ap energy levels remain unpopulated by FP529F/Y.

Fig. 3 *C* shows the effect of replacing an *L* residue with an *R* at position 527. Once again, ΔG_{tb-fi} is unaffected by the mutation, but the sa, pi, and ap conformations are all stabilized relative to the fi state. Of these three conformational states, the sa state has the lowest Gibbs energy, even though the pi state has the lowest internal energy. This once again indicates that peptide segments in the bilayer interface have much greater entropy than those inserted into the interior and reaffirms the importance of entropy in overall conformational stability. The entropies of the two pi states (529pi and 527pi) are effectively the same ($\Delta S_{pi-fi} = 44$ and 43 cal/mol/K, respectively), suggesting that the slightly different tethering point is not an important factor in the overall flexibility of the peptide chain.

Fig. 3 *D* shows the effect of deleting seven residues from the N terminus (hydrophobic tail) of FP. The shortened peptide can no longer easily span the bilayer, so the Gibbs energy of the tb state is very high, and the state is unpopulated. The pi state is also unpopulated, being insufficiently stabilized by the deletion. The sa and ap conformational states of FPCLP1, in contrast, are considerably more stable than their FP counterparts. These states have about the same Gibbs energy, and are therefore populated to about the same extent. For both states, a comparison of ΔS_{sa-fi} and ΔS_{ap-fi} for FP527L/R and FPCLP1 suggests a simple, linear relationship between ΔS and the number of virtual bonds linking each model residue, n_v. $\Delta S_{sa-fi} \sim 5.3\ n_v$ cal/mol/K and $\Delta S_{ap-fi} \sim 6.1\ n_v$ cal/mol/K.

DISCUSSION

After initial adsorption, the model FP peptide inserts deeply and obliquely into the bilayer, almost exclusively residing in this fi conformational state, in agreement with Fourier transform infrared and electron spin resonance studies (Martin et al., 1996; Gordon et al., 1992). Our model also predicts an average angle of insertion of 38° in close agreement with the 40° angle suggested by Gordon et al. (1992) and the 41° angle based on the hydrophobic moment plot analysis of Brasseur et al. (1990). Martin et al. (1996) also suggest an insertion angle of 40° for the closely related SPwt and SP-2 peptides. In addition, our simulations of FP527L/R agree with the analysis of Mobley et al. (1999), which suggests that the L/R replacement reduces the depth to which this peptide penetrates the bilayer interior.

However, unlike previous experimental studies, we also observed FP in the *tb* conformational state, even after the system had fully equilibrated. Because this conformational state is only observed in 2% of our system configurations, it is unlikely to be noticed by Fourier transform infrared or electron spin resonance, where data are averaged over all peptide configurations. The FP variant peptides also exhibit more than one stable conformation at equilibrium (FP527L/R partitions between six distinct states). Great care must therefore be taken when probing the membrane conformations of these peptides using averaging experimental methods. Although averaged conformations might suggest that each variant inserts in a unique conformation, slightly different to all the others, our analysis provides a very different picture. We find that the peptides partition between a small number of common conformational states, and that it is the partitioning that changes upon mutation. This radically different picture of peptide mutant behavior may help to explain the changes in activity and functionality exhibited by mutated versions of active fusion peptides such as FP. To illustrate this point, we have modeled the same series of peptides that were studied by Mobley et al. (1999), who quantified the functional activity of FP variants for human red blood cell (RBC) hemolysis and aggregation through a series of experiments. Our conformational partitioning data, combined with their activity measurements, provide important mechanistic insights, as outlined below.

Although the inducement of positive curvature at the membrane surface is often associated with membrane lysis (Epand and Epand, 2000), Mobley et al. (1999) propose a different mechanism for RBC hemolysis. They suggest a mechanism involving negative curvature at the membrane surface as a result of deep and oblique peptide insertion. Surface-adsorbed peptides, which tend to increase the positive curvature at the surface, should therefore be important in the mechanism described by Epand and Epand, whereas

TABLE 5 A comparison of the relative aggregation activity of FP and its variants with the simulated partitioning of each peptide into the sa conformational state

	RBC aggregation	sa %
FP	100	0
FP520V/E	51	1
FP529F/Y	35	1
FP527L/R	0	19
FPCLP1	0	24

peptides that penetrate deeply into the bilayer interior, and are tilted away from the bilayer normal, should be important in the mechanism suggested by Mobley et al. (Epand and Epand, 2000; Bradshaw et al., 2000).

Our results show no correlation between surface adsorption and RBC hemolysis. In fact, although FP is the most hemolytically active peptide considered, it does not partition into the sa conformational state at all. In contrast, FP527L/R and FPCLP1, which show greatly reduced hemolytic activity, have the highest proportion of sa conformers. These data therefore do not support a hemolysis mechanism involving surface-adsorbed peptides.

However, there is evidence to support the negative curvature mechanism suggested by Mobley et al. For each FP variant, there is a reduction in the depth of insertion (FPCLP1), angle of insertion (FP520V/E), or proportion of deeply and obliquely inserted conformers (FP529F/Y and FP527L/R), relative to FP. According to the negative curvature mechanism, each of these changes in insertion behavior should cause a reduction in hemolytic activity, and the experimental data shows just such a correlation (Mobley et al., 1999; Table 2). Our partitioning analysis, therefore, supports the negative curvature mechanism for RBC hemolysis by FP.

Our simulations of FP and its variants also show a correlation (Table 5) between the presence of surface-adsorbed peptide conformations ($>1\%$) and the blocking of RBC aggregation (Mobley et al., 1999; Table 2). Peisajovich et al. (2000) found that a charged, hydrophilic peptide that protrudes from the surface of a bilayer, inhibits bilayer-bilayer contact and consequently the formation of the hexagonal phase, which requires many points of contact between bilayer surfaces. As noted earlier, the sa conformational state of our model peptide includes conformations in which the charged hydrophilic end protrudes from the bilayer surface in a similar manner. Therefore, FP527L/R and FPCLP1, which are $\sim 20\%$ partitioned into the sa conformational state, would be expected to have a small but significant population of charged hydrophilic segments protruding from the surface at any given time. Although this may not seriously hinder fusion, which requires only one point of contact between bilayers, it appears to be a sufficient deterrent to aggregation, which, like hexagonal phase formation, requires many points of contact between bilayer surfaces.

Although Mobley et al. (1999) also reported lipid mixing (fusion) activities for each of the peptides tested, it is not clear that the fluorescence quenching technique used by them and by several other groups (Martin et al., 1996; Pereira et al., 1997; Peisajovich et al., 2000) actually demonstrates vesicle fusion. Because fusion is a complex process, which may be better studied with reference to cell fusion experiments involving the entire gp41 glycoprotein, it will not be discussed here. However, cell fusion experiments have been reported for the mutated FPs described by Mobley et al. (Freed et al., 1990; Bergeron et al., 1992; Schaal et al., 1995) as well as for several other peptide variants (Felser et al., 1989; Cao et al., 1993). In addition, the dominant interference effects of mutants on the activity of the wild-type FPs have also been reported (Freed et al., 1992; Buchschacher et al., 1995; Schaal et al., 1995). These data will be addressed in a later publication in which we will investigate the relationship between cell fusion activity and FP conformations and conformational partitioning.

CONCLUSIONS

We have previously demonstrated the accuracy of our model peptide/membrane system and Monte Carlo simulation technique in reproducing the insertion behavior of two subtly different peptides, M2δ and Magainin2 (Maddox and Longo, 2002). Here we have shown that the model may also be applied to other short peptide chains with similarly impressive results. In particular, FP, the N-terminal peptide of HIV-1 glycoprotein gp41 has been studied by several groups using different experimental and theoretical techniques (Gordon et al., 1992; Brasseur et al., 1990; Martin et al., 1996; Mobley et al., 1999). Our simulations predict an angle and depth of insertion almost identical to those observed and predicted previously. In addition, where information is available regarding the insertion behavior of FP mutagens, for example the reduction of the average depth of insertion of FP527L/R relative to FP (Mobley et al., 1999), our model shows the same effect. These results offer further evidence of the general use of our model, model parameters, and simulation technique in the study of peptide interaction with phospholipid bilayers.

Having further established the validity of our model and its ability to reproduce measurable, experimentally observed behaviors, we have made use of one of the most important aspects of molecular simulation, the readily accessible data on everything from atomic (or molecular) coordinates to internal energy. Analysis of these data led to the unexpected conclusion that peptides often partition between multiple distinct conformations within a membrane, rather than predominantly occurring in just one stable state, as seems to be generally assumed. Such a conclusion, if verified experimentally, could substantially change the interpretation of data regarding peptide-induced cell processes such as lysis, aggregation, and fusion.

A second surprising observation regarding partitioning is that none of the peptides we studied had its own unique set of conformational states. Instead, most conformations were common to more than one of the peptides considered so that even after replacing a residue, or deleting several residues, a peptide variant still spends much of its time in the same fi state as wild-type FP. Rather than shifting to a completely different conformation as previously assumed, or shifting to a completely different set of conformations, the mutation of FP merely causes a shift in the conformational partitioning between a small set of conformational states.

Such a picture of the conformational distribution of peptides within a bilayer can provide new insights into important cell processes. Here we have used our partitioning data to support a mechanism for human RBC hemolysis involving negative membrane curvature and to suggest that protruding, charged segments of sa peptides may provide a slight repulsion between membrane surfaces, blocking RBC aggregation.

Finally, our partitioning data illustrate the importance of entropic differences in determining the relative stabilities of alternative conformations. For example, on purely energetic grounds (internal energy), the *tb* conformation of FP is more stable than the fi conformation. However, the greatly increased entropy of the fi form tips ΔG in its favor, and it is this conformation that dominates the insertion behavior of FP. To our knowledge, this is the first time any attempt has been made to assess the relative entropies of peptide conformations in a lipid bilayer.

We have shown that computer simulations allied with good theoretical models are not merely predictive in nature, but can be extremely useful tools for the understanding and analysis of experimental data, providing a microscopic picture to help explain macroscopic observations. Furthermore, although the commonly used full-atom molecular dynamics simulation method can provide a more detailed picture of essentially static systems than our simplified model, it is unable to probe long timescale properties of peptide/membrane systems. One such property, conformational partitioning could therefore only have been observed by a long timescale technique such as our simplified Monte Carlo simulation. This type of simulation is therefore an excellent complimentary technique to full-atom molecular dynamics and an essential addition to the theoretician's armory for the study of all aspects of peptide/membrane behavior.

This work was supported by the National Science Foundation through the CAREER Program (BES-9733764) and the Materials Research Science and Engineering Center program of the National Science Foundation under Award DMR-9808677. We also wish to acknowledge Joe and Essie Smith, whose generous gift helped to fund this work.

REFERENCES

Bergeron, L., N. Sullivan, and J. Sodroski. 1992. Target cell-specific determinants of membrane fusion within the human immunodeficiency virus type 1 gp120 third variable region and gp41 amino terminus. *J. Virol.* 66:2389–2397.

Bradshaw, J. P., M. J. Darkes, T. A. Harroun, J. Katrsaras, and R. M. Epand. 2000. Oblique membrane insertion of viral fusion peptide probed by neutron diffraction. *Biochemistry.* 39:6581–6585.

Brasseur, R., M. Vandenbranden, B. Cornet, A. Burny, and J. M. Ruysshaert. 1990. Orientation into the lipid bilayer of an asymmetric amphipathic helical peptide located at the N terminus of viral fusion proteins. *Biochim. Biophys. Acta.* 1029:267–273.

Buchschacher, Jr., G. L., E. O. Freed, and A. T. Panganbian. 1995. Effects of second-site mutations on dominant interference by a human immunodeficiency virus type 1 envelope glycoprotein mutant. *J. Virol.* 69: 1344–1348.

Cao, J., L. Bergeron, E. Helseth, M. Thali, H. Repke, and J. Sodroski. 1993. Effects of amino acid changes in the extracellular domain of the human immunodeficiency virus type 1 gp41 envelope glycoprotein. *J. Virol.* 67:2747–2755.

Epand, R. M., and R. F. Epand. 2000. Modulation of membrane curvature by peptides. *Biopolymers.* 55:358–363.

Felser, J. M., T. Klimkait, and J. Silver. 1989. A syncytia assay for human immunodeficiency virus type 1 (HIV-1) envelope protein and its use in studying HIV-1 mutations. *Virology.* 170:566–570.

Freed, E. O., E. L. Delwart, G. L. Buchschacher, and A. T. Panganiban. 1992. A mutation in the immunodeficiency virus type 1 transmembrane glycoprotein gp41 dominantly interferes with fusion and infectivity. *Proc. Natl. Acad. Sci. U. S. A.* 89:70–74.

Freed, E. O., D. J. Myers, and R. Risser. 1990. Characterization of the fusion domain of the human immunodeficiency virus type 1 envelope glycoprotein gp41. *Proc. Natl. Acad. Sci. U. S. A.* 87:4650–4654.

Gordon, L. M., C. C. Curtain, Y. C. Zhong, A. Kirkpatrick, P. W. Mobley, and A. J. Waring. 1992. The amino-terminal peptide of HIV-1 glycoprotein gp41 interacts with human erythrocyte membranes: peptide conformation, orientation and aggregation. *Biochim. Biophys. Acta.* 1139: 257–274.

Griffith, O. H., P. H. Dehlinger, and S. P. Van. 1974. Shape of the hydrophobic barrier of phospholipid bilayers (evidence of water penetration). *J. Membr. Biol.* 15:159–192.

Maddox, M. W., and M. L. Longo. 2002. A Monte Carlo study of peptide insertion into lipid bilayers: equilibrium conformations and insertion mechanisms. *Biophys. J.* 82:244–263.

Martin, I., H. Schaal, A. Scheid, and J. Ruysschaert. 1996. Lipid membrane fusion induced by the human immunodeficiency virus type 1 gp41 N-terminal extremity is determined by its orientation in the lipid bilayer. *J. Virol.* 70:298–304.

Mobley, P. W., A. J. Waring, M. A. Sherman, and L. M. Gordon. 1999. Membrane interactions of the synthetic N-terminal peptide of HIV-1 gp41 and its structural analogs. *Biochim. Biophys. Acta.* 1418:1–18.

Peisajovich, S. G., R. F. Epand, M. Pritsker, Y. Shai, and R. M. Epand. 2000. The polar region consecutive to the HIV fusion peptide participates in membrane fusion. *Biochemistry.* 39:1826–1833.

Pereira, F. B., F. M. Goñi, A. Muga, and J. L. Nieva. 1997. Permeabilization and fusion of uncharged lipid vesicles induced by the HIV-1 fusion peptide adopting an extended conformation: dose and sequence effects. *Biophys. J.* 73:1977–1986.

Roseman, M. A. 1988. Hydrophilicity of polar amino acid side-chains is markedly reduced by flanking peptide bonds. *J. Mol. Biol.* 200:513–522.

Schaal, H., M. Klein, P. Gerhmann, O. Adams, and A. Scheid. 1995. Requirement of N-terminal amino acid residues of gp41 for human immunodeficiency virus type 1-mediated cell fusion. *J. Virol.* 69: 3308–3314.